

Detection of Conductive Lane Markers using mmWave FMCW Automotive Radar

Austin Greisman, Keyvan Hashtrudi-Zaad, and Joshua A. Marshall

Abstract—Localization of vehicles in inclement weather conditions, including snow and heavy rain, is a significant issue plaguing autonomous vehicle systems. Our work takes a step towards tackling this problem by leveraging existing hardware commonly used in self-driving vehicles, namely low-cost millimetre wave (mmWave) radar systems to detect conductive paint on roads. This paper presents the results of preliminary experiments that indicated that, even with full snow coverage of the conductive paint, the radar system is still able to successfully detect the material as a potential marker for lateral vehicle localization.

I. INTRODUCTION

Autonomous vehicles are an emerging industry that still needs new technology to achieve full Level 5 autonomy. Level 5 autonomy, as stated by the Society of Automotive Engineers (SAE), refers to a completely autonomous driving system with no needed intervention from a human driver in all conditions [1]. By allowing for a completely autonomous experience, the safety of the human driver would drastically increase. A study performed by Tesla from 2016 to 2019 showed that their autopilot system caused users to experience $7\times$ fewer accidents than non-auto-pilot drivers [2]. Keep in mind, this is with an autonomous vehicle system ranked at SAE Level 2. One aspect hindering autonomous vehicles is their ability to localize in poor weather conditions, like heavy rain or snow.

This paper explores a novel solution that uses Frequency Modulated Continuous Wave (FMCW) Automotive radar to help localize autonomous vehicles on urban roads or highways in all weather conditions. Practitioners separate this problem into two distinct sections, longitudinal, and lateral localization. This research focuses solely on lateral localization. Current localization systems utilize a combination of sensors: cameras, which do not work under many adverse weather conditions; GPS, which is nominally accurate to within 7.3 m 95% of the time in ideal conditions and are prone to a shadowing effect [3], [4]; ultrasonic sensors, which localize with respect to neighbouring cars with limited accuracy in adverse weather; and, LiDAR, which is not able to detect road identifiers underneath cover. However, radar has the potential to remain useful in most adverse weather conditions [5], including snow, rain, and fog.

Section I of this paper discusses challenges autonomous vehicles face with localization, followed by the current re-

The authors are with the Department of Electrical and Computer Engineering and the Ingenuity Labs Research Institute, Queen's University, Kingston, ON K7L 3N6 Canada, austin.greisman@queensu.ca.

This work was supported in part by the Natural Sciences and Research Council of Canada (NSERC) under grant RGPIN-2015-04025, a Mitacs Research Training Award (RTA), and the Vector Institute.

search that attempts to solve these problems in different ways, which serves as the motivation behind our proposed approach. Section II focuses on the theory behind our radar-based method, including details about how parameters are gleaned from the radar unit and technical details related to our experimental results. Section III details our experimental set up, followed by Section IV that provides an in-depth analysis of the gathered results. Section V draws conclusions and suggests future work.

A. Current Research

Using millimetre wave radar (30–300 GHz) to improve approximate localization under poor weather conditions has become a popular method for autonomous vehicles. Some researchers have found success by fusing different sensors including LiDAR, cameras, and ultrasonic with radar. Yoneda *et al.* [6] performed testing to compare LiDAR and omnidirectional radar at 76 GHz in poor weather conditions by using relative RMS value errors. Radar consistently had an RMS value of ≈ 0.25 m in snowy conditions, while the LiDAR RMS error fluctuated widely between ± 1 m. Ward *et al.* [7] attempted sensor fusion by using low-cost radar sensors; namely, off-the-shelf automotive radar units for use in areas with limited GPS. Radar, cameras, and LiDAR have also been used with Iterative Closest Point (ICP) and Extended Kalman Filter (EKF) algorithms. Their results showed similar performance compared to more complex methods that have access to a larger dataset.

Zhang [8] proposed a novel method using FMCW 76 GHz automotive radar's Range Doppler plot for terrain and target mapping, which showed promising localization and identification potential. Asuzu *et al.* [9] and Viikari *et al.* [10] both performed backscattering analysis on asphalt for the detection of different road conditions, including dry, rainy, snowy, and slushy. Both their results showed successful differentiation among various features. However, all localization methods continue to have issues with positioning in snowy and heavy rain conditions. These methods improve the current result, but not significantly enough for a jump in the levels of autonomy. Radar is usually used as an additional sensor to improve accuracy, but not as the main sensor in itself [7], [8]. Consequently, all of the above-mentioned methods, other than [7], [8], use custom full front-end equipment that requires expensive equipment. The research described in this paper uses low-cost automotive radar in the range of \$300.00 USD.

B. Motivation

Radar technology has been installed in commercial vehicles since 1992 [5]. As the technology has become more affordable, many manufacturers have begun to install radar units at all four corners of vehicles behind the bumpers, as well as at other locations [11]. Radar data is naturally sparse in comparison to LiDAR or camera information and is, therefore, more difficult to use as a substitute. Due to the lower frequency spectrum of radar when compared to vision based systems, atmospheric and weather conditions that would normally blind a vision system do not affect radar significantly over short distances.

By using the pre-installed radar systems, we theorized that reflected radar "chirps" could be used to triangulate specific material differences between asphalt and concrete when compared to road-specific paints like Poly(methyl methacrylate) (PMMA). However, after extensive testing, it was determined that the conductivity differences at automotive frequencies between PMMA and asphalt were too insignificant to be detectable from surrounding noise. Therefore, to increase the detectable conductivity differences between the asphalt and paint, we introduced particulate ferrous metal particles into the paint that would then be used for lane markers. This new approach changes the expected response of the radar unit to have significant spikes in reflected radar gain at the specific areas where the metallic paint has been applied. However, this is only true for a radar unit that is nearly parallel to the conducting surface. Yet, it might be used to identify lanes, which is the focus of the research presented by this paper.

II. THEORY

For the studies presented by this paper we used a Texas Instrument (TI) AWR1443BOOST module with an attached DCA1000EVM ADC Collection board. The AWR1443 operates between 77 to 81 GHz using a FMCW system setup. During testing, the full bandwidth of the radar unit was used. This frequency ramp allows for subtraction of the sent wave, also called a *chirp*, to the returned wave to glean the *beat frequency*, f_B . The beat frequency is made up of complex numbers called *I/Q data*. One f_B collected multiple times over a cyclic period is called a *frame*. By organizing the collected data into a 3D grid, as shown in Fig. 1, a 2D Fast Fourier Transform (FFT) can be applied to the data, layer by layer, to extract relative range and velocity information. Parameters M , L , and N represent the total number of *chirps*, the total number of *I/Q* data samples collected in each *chirp*, and the number of RX antennas, respectively. Detected objects have their azimuth and elevation angle calculated by performing an FFT across the antennas at that specific object.

In our research, we studied the use of radar to detect ferrous particles in metal paint as a potential technique for localizing lanes on asphalt roadways. The underlying physics behind this process lies with the conductivity of the paints in comparison with that of a dielectric like asphalt. Since the differences are so stark, the radar reflection would be significantly different when the wave strikes a conductive

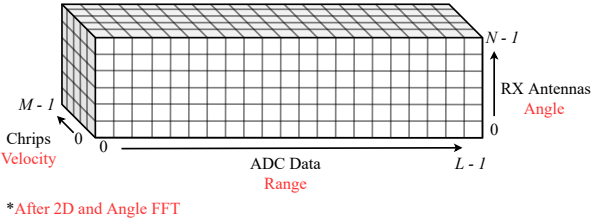


Fig. 1. 3D Data storage matrix for gathered *I/Q* data (ADC Data) and post FFT data. Chirps represent the independent signals received from the environment after transmission. Each antenna receives each of the same chirp at slightly different times, which are then stacked on top of each other allowing for a 3D Matrix. By performing a 3D FFTs, the peaks of the detected objects allow for accurate estimation of positions, velocities, and angles.

surface versus a non-conducting one. We can observe this by looking at the reflection coefficient of the material in question

$$\Gamma = \frac{\eta_1 - \eta_0}{\eta_1 + \eta_0}, \quad (1)$$

where Γ is the reflection coefficient of a material [12], η_1 is the impedance of the material in question, and $\eta_0 = 377 \Omega$ is the impedance of air [12]. The rationale behind this is that we assume the system is facing towards the ground with either magnetite, asphalt, or snow and magnetite in its path. Snow is omitted in this example for simplicity, however, the result would be the same due to the difference between water conductivity compared to that of magnetite.

Let's use magnetite as an example since its presence is verified in two of our tested paints. We can use the simplified impedance equation

$$\eta_1 = (1 + j) \sqrt{\frac{\pi f \mu_r \mu_0}{\sigma}}, \quad (2)$$

where μ_r , f , and σ are the relative permeability, frequency of the wave, and conductivity of the material respectively. $\mu_0 = 4\pi \times 10^{-7} \frac{H}{m}$ as the permeability of free space [12]. Equation (2) can only be used if the material satisfies this condition of the loss tangent,

$$\frac{\varepsilon''}{\varepsilon'} = \frac{\sigma}{2\pi f \varepsilon_r \varepsilon_0} > 100 \quad (3)$$

where ε' , ε'' , ε_r , ε_0 equal the real permittivity, imaginary permittivity, relative permittivity, and permittivity of free space respectively. Magnetite has the following Electromagnetic (EM) parameters, $\mu_r \approx 16 \frac{H}{m}$, $\sigma \approx 1 \times 10^5 \frac{S}{m}$, and $\varepsilon' = \varepsilon_r \varepsilon_0 \approx 17 \frac{F}{m}$ at a f of 79 GHz [13], [14]. Parameter f was selected as it is the average frequency used by the unit. By plugging in the aforementioned values into (3), magnetite is then confirmed as a good conductor. We obtain the follow value for magnetite's impedance by using (2),

$$\eta_1 = (1 + j)7.06 \Omega. \quad (4)$$

Therefore, by substituting the impedance for air and magnetite into (1) we obtain the magnetite reflection coefficient as

$$\Gamma_M \approx \frac{7.06 \Omega - 377 \Omega}{7.06 \Omega + 377 \Omega} = -0.96. \quad (5)$$

TABLE I
CONCENTRATION AND PAINT MAKEUP OF EACH PAINT TESTED.

Manufacturer	Metal	Paint Base	Concentration of Metal
SmartSurfaces	Magnetite	Water	55%
SmartSurfaces	Magnetite	Water	60%
MagnaMagic	Iron	Latex	Unknown

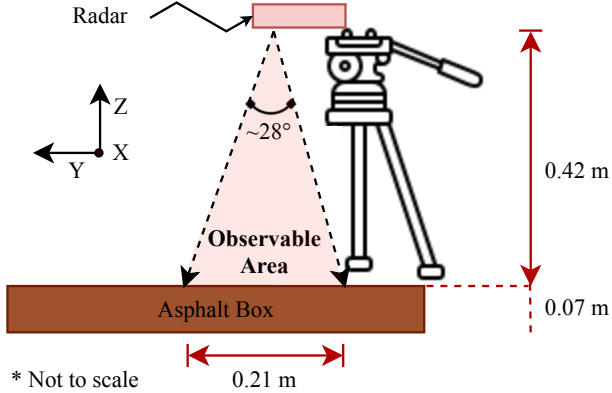


Fig. 2. Illustration of 3 dB elevation angle observable area of the radar unit. The observation area angle was determined from the AWR1443BOOST datasheet, where plots of the gain intensity vs. angle away from the boresight were plotted.

Since asphalt is considered a low-loss medium, the impedance of asphalt is found by

$$\eta_1 = \sqrt{\frac{\mu_r \mu_0}{\epsilon_r \epsilon_0}}, \quad (6)$$

which is used instead of (2) [12]. Computing Γ_A for asphalt by using (6) with $\mu_r \mu_0 \approx 1.26 \times 10^{-6} \frac{H}{m}$, $\sigma \approx 10^{-2} \frac{S}{m}$, and $\epsilon_r \epsilon_0 \approx 3.98 \times 10^{-11} \frac{F}{m}$, we obtain [15]–[17]

$$\Gamma_A = \frac{177.6 \Omega - 377 \Omega}{177.6 \Omega + 377 \Omega} \approx -0.36. \quad (7)$$

Comparing (5) with (7) shows the drastic difference in reflectivity. Magnetite with its high conductivity compared to asphalt allows for a large portion of the incident wave to be reflected off of the surface, while asphalt only reflects approximately 36% of the energy back, ideally.

III. EXPERIMENTAL SETUP

The conductivity differences between dielectrics (asphalt) and metals is sufficiently large; therefore, ferrous material is needed [18]. For simplicity and initial testing, metal paint from the companies SmartSurfaces and MagnaMagic with different metal concentrations were acquired for comparison. This was instead of mixing and creating our own paint for testing. The paint makeups can be seen in Table I.

The AWR1443BOOST was attached to a tripod and a PhidgetSpatial Precision 3/3/3 Inertial Measurement Unit (IMU) for measuring the angle of inclination relative to the ground. Fig. 2 illustrates the observable area of the radar unit.

A 63 cm by 90 cm by 5 cm deep wooden box was created as a simulated road to house cold asphalt, Fig. 3. Since the



Fig. 3. Outdoor testing setup with no painted strips present.



Fig. 4. 0.1 m × 0.86 m × 0.02 m cardboard mold for metal paint.

frequency spectrum used by the AWR1443 is between 77 to 81 GHz, the skin depth equation for electromagnetic waves was used to determine the optimum depth for the asphalt testing rig so that any material underneath the rig would not affect the test. Skin depth is determined with $\delta = \frac{1}{\alpha}$, where δ is the skin depth of an electromagnetic wave propagating into a solid and α is the attenuation constant of the material. In the case of asphalt, $\alpha \approx 54 \frac{N_p}{m}$, which equates to $\delta \approx 1.85$ cm [19]. However, it should be noted that α was determined when the EM wave frequency was approximately 94 GHz and with asphalt containing 85% small rock particulate content. Only pure cold-asphalt (bitumen) was used in this experiment. The box depth was built to 5 cm of bitumen depth and, as mentioned previously, the conductivity differences between dielectrics (asphalt/bitumen) and conductors is significant.

A mould was created, as seen in Fig. 4, to evenly distribute each paint, 2 mm thick onto a 10 cm width section of the bitumen setup. In Ontario, Canada, where the experiment was taken place, centre road lines are 1.9 ± 0.4 mm thick by 10 cm wide [20]. We attempted to replicate this thickness in our



Fig. 5. Outdoor testing setup with a painted strip present.

experiments with limited success, the paints were quite thick and difficult to evenly distribute. Therefore, our painted line thicknesses were approximately 1.5 ± 0.7 mm.

Testing involved three separate experiments, each with nine horizontal shifts at -8 cm, -6 cm, -4 cm, -2 cm, 0 cm, 2 cm, 4 cm, 6 cm, 8 cm. A baseline measurement of the unpainted asphalt box was first taken, as shown in Fig. 3. The shifts presented were to obtain a greater sweep of values since radar data is naturally sparse. The increment of -2 cm was chosen in order to have the radar unit over top of the paint for approximately three of the nine samples. Next, the three different paints were placed onto the asphalt. The SmartSurfaces 60% concentration of magnetite test can be seen in Fig. 5. Finally, snow was laid atop the asphalt in an even distribution of approximately 5 ± 2 cm of light snow, as is shown in Fig. 6.

The radar unit was mounted on top of the tripod connected to a Intel Core i5 540M / 2.53 GHz Lenovo ThinkPad T410 for data collection. The system was then calibrated for approximate receive power from incoming chirps by using a sheet of aluminium 0.42 m away from the unit. The peak FFT values for each received detected angle were passed through the following equation, which has been verified by the radar manufacturer to allow for an approximate receive power [21],

$$G_{\text{dBm}} = 10 \log \left(\frac{f_p}{G_{\text{RFFT}} G_{\text{VFFT}} G_{\text{AFFT}}} \right) - G_{\text{RX}} \quad (8)$$

$$RX_{\text{POW}} = 10^{\frac{G_{\text{dBm}}}{10}}, \quad (9)$$

where f_p is the calculated peak FFT value for each angle, and G_{RFFT} , G_{VFFT} and G_{AFFT} represent the FFT gain applied to the signal for the range, velocity, and angle during the FFT calculations, respectively. The parameter G_{RX} is the gain applied by the system to the signal after being received by the antennas. RX_{POW} is the final estimated receive power of the system at that angle. The output power from the system at the ball was found to be 15 mW, as stated in the AWR1443BOOST data sheet. However, the actual power



Fig. 6. Outdoor testing setup with approximately 5 ± 2 cm of snow on top of the painted strip.

TABLE II
DIFFERENT AVAILABLE RADAR PROFILES FOR AWR1443BOOST WITH CORRESPONDING DATA VALUES. ALL VALUES ARE APPROXIMATED.

Profile	FOV _{3dB}	Angle Resolution
3D 3TX, 4RX	H $\pm 28^\circ$, E $\pm 14^\circ$	14° , 28°
2D 2TX, 4RX	H $\pm 28^\circ$, E $\pm 14^\circ$	14°
2D 1TX, 4TX	H $\pm 28^\circ$, E $\pm 14^\circ$	29°
2D 1TX, 2RX	H $\pm 28^\circ$, E $\pm 14^\circ$	57°

transmitted by the antenna network was not mentioned in any documentation. Therefore, the output power was estimated to be approximately 15 mW as during testing with Aluminum, the RX_{POW} calculated was approximately 14.4 mW.

A. Testing Plan

The testing was separated into two distinct sections. Initially, the static parameters are presented, then the changing parameters.

Constants:

- 1) Thickness of paints is approximately 1.5 ± 0.7 mm.
- 2) Testing will be done outdoors.
- 3) 8 samples (frames) of each test will be performed.
- 4) Only the 2D AWR1443 Profile will be used.
- 5) Radar tilt will be 180° relative to the ground.

Variable Parameters:

- 1) Radar will be inline with the paint for testing, then shifted by -8 cm, -6 cm, -4 cm, -2 cm, 0 cm, 2 cm, 4 cm, 6 cm, and 8 cm.
- 2) Three different magnetic paints shall be tested.

As previously mentioned, the paint thickness was chosen to replicate Ontario, Canada's road marker paints [20]. Outdoor testing was necessary since Queen's Ingenuity Labs Research Institute was closed due to the COVID-19 pandemic. Eight frames were chosen arbitrarily since it was the default number provided by the radar manufacturer. We observed that increasing the number of frames taken per sample did not improve accuracy as the system was highly consistent with its

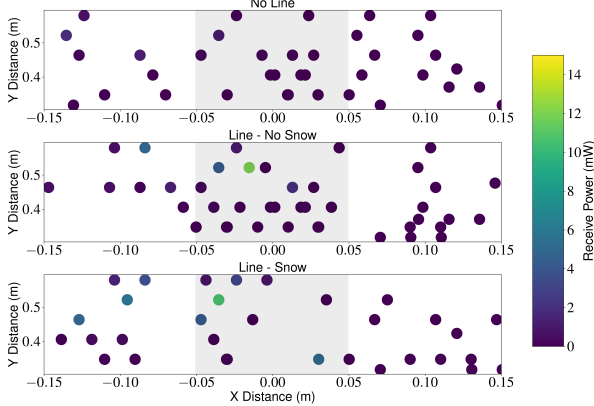


Fig. 7. Points detected relative to AWR1443 in all three testing cases based on the **55% magnetite** concentration used. Subplot one is a baseline asphalt test with no paint present. The second subplot has a painted line, but with no snow. The final subplot has snow on top of the painted lines. During the two last subplots, the painted lines were placed approximately between the -0.05 m and 0.05 m area displayed in each figure, which has been shaded.

results for each frame. Due to time constraints, only the 2D AWR1443 profile was implemented during testing. The other available profile configurations can be viewed in Table II. A radar tilt of 180° relative to the ground was mandatory due to the aforementioned reflection angle expected from the signal.

IV. RESULTS AND ANALYSIS

The experimental results are shown in Figs. 7, 8, and 9. Each figure represents a combination of data taken over the aforementioned offsets with eight separate frame measurements per sample. All plots are 3D representations of what the radar unit observed in each test. The x -direction corresponds with the horizontal displacement of points relative to the radar unit, while the y -direction corresponds to the vertical displacement of points relative to the radar unit, which was pointed directly down and parallel to the ground. This is shown in Figs. 3, 5, and 6. The colour of each point corresponds to the estimated receive power, which would inform the viewer if a material with a high reflection coefficient was struck and received by the radar unit. A 0.3 m to 0.6 m section in the y -direction was cropped since the radar unit was 0.42 m above the asphalt and all other data could be interpreted as noise.

The first subplot in each figure illustrates the baseline asphalt test previously mentioned. The second subplot are the tests performed while no snow was present, but the paint lines were. The final subplot has snow on top of the painted lines, rendering them unseen in the visual spectrum. During the other two tests, the painted lines were placed approximately between the -0.05 m and 0.05 m area displayed in each figure.

The significance of the conductive paint lines can be seen in all results. During each test, when the radar unit was directly above the painted line, with or without snow, a strong reflection was recorded indicating the relative position of the line. The other points surrounding the high $RXPOW$ points indicate the relative low reflective power of snow and asphalt (both dielectrics) compared to 55% and 60% magnetite.

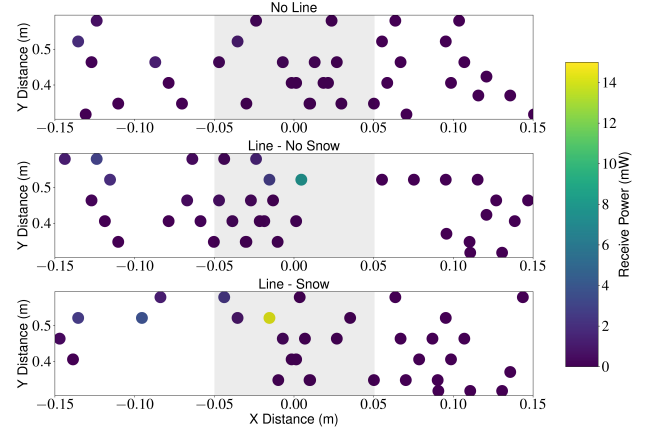


Fig. 8. Points detected relative to AWR1443 in all three testing cases based on the **60% magnetite** concentration used. Subplot one is a baseline asphalt test with no paint present. The second subplot has a painted line, but with no snow. The final subplot has snow on top of the painted lines. During the two last subplots, the painted lines were placed approximately between the -0.05 m and 0.05 m area displayed in each figure, which has been shaded.

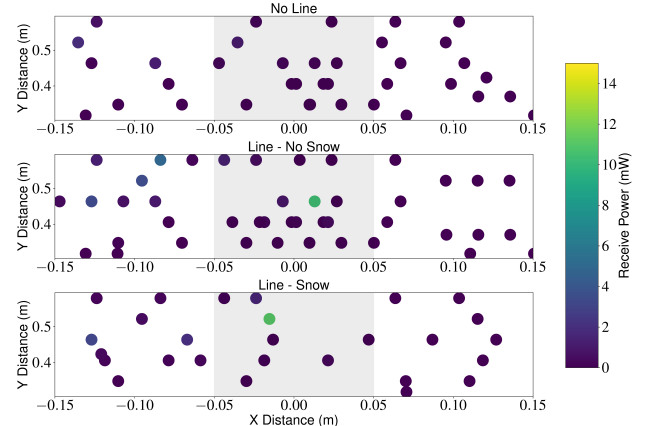


Fig. 9. Points detected relative to AWR1443 in all three testing cases based on the **MagnaMagic paint** with unknown concentration. Subplot one is a baseline asphalt test with no paint present. The second subplot has a painted line, but with no snow. The final subplot has snow on top of the painted lines. During the two last subplots, the painted lines were placed approximately between the -0.05 m and 0.05 m area displayed in each figure, which has been shaded.

It should be noted that, as shown in Fig. 8, the reflected power—where the painted line was detected—was higher than the estimated power received where no snow was present. We believe this is due to the extremely sensitive nature of the incident and reflected waves created by the radar unit off of the paints. It is highly likely that during testing, the radar unit was not as level as the snow-covered test cases, which is where the discrepancy appears. Since the receive antenna area is only approximately 0.442 cm^2 , the available area for the signal to return to the unit is small while a majority of the energy reflected off of the paint. The painted lines were also not perfectly level when dried due to a lack of available equipment as a result of the COVID-19 pandemic.

Since the wavelength of the radar unit during testing was

approximately 3.8 mm (79 GHz), due to the microscopic size of the metallic particles in each paint, the majority of the transmitted chirps would reflect off of the conductive paint with the same angle of inclination. Therefore, the experimental results prove that if the radar unit was not near-perfectly level with the paint and ground, the reflectively intensity would be significantly diminished. However, if near-perfectly inline with the ground, the response back is significant.

The efficacy of the system with a perfectly flat conductor, like aluminum foil, is 100%. With the proper equipment, the painted lines would have the same efficacy based on the gathered results. However, the effectiveness degrades when additional material is in-between the conductor and the radar unit. These results correlate with the limits imposed by the estimated receive power and Continuous False Alarm Rate (CFAR) for this system.

The software used to process the results was created in Python. The data was initially collected from the radar unit using TI's Radar Studio software. The received data was in binary format and was then translated to int16 complex numbers. These numbers were then imported into the final python script, which contains system parameters such as bandwidth, frequency ramp slope, RX gain, sample rate, number of chirps, number of frames, and number of complex numbers per chirp. These values were then used after performing a 3D FFT on the data to glean position, velocity, and angle data. Plots were then created using *matplotlib* to display the data.

V. CONCLUSION

Theoretical and experimental analyses were done to determine the potential for low-cost automotive FMCW radar units to be used as a method for localization in the presence of conductive materials on asphalt. To the best of our knowledge, this is a new development that has not been reported in the literature. This paper provides a high-level breakdown of the calculations involved in manipulating the incoming RX data, with a reflectively coefficient example to theoretically justify the expected results. The experimental setup and test cases are described, followed by an in depth review of the data collected. The results provide experimental evidence that detecting conductive paint lane markers with radar, when sensors such as LiDAR, cameras, or ultrasonic may not be able to identify, is indeed a possibility. Further development of this method is needed so that the technique might be implemented into existing autonomous vehicle systems.

Future work will aim to determine which materials or combinations of materials allow for localization using low-cost radar at angles other than 180° relative to the ground. One area that we plan to investigate is the use of road reflectors, which are already utilized on many major Canadian highways and in other jurisdictions around the world. More tests are needed with varying thicknesses of snow and snow densities to test the limits of the method. The current system uses a 2D angle method, which does not allow for x , y , and z data input. Another next step will be to implement this method for a more comprehensive range of reflected points

off of the conductive material under test. Finally, such a system would only be useful for a vehicle that is moving, not stationary. Doppler compensation to the angle data will need to be added to the custom algorithm developed in this paper to allow for stationary conditions, accompanied by testing of localization accuracy in motion. Nevertheless, we believe that the preliminary results presented in this paper are promising.

REFERENCES

- [1] S. international, "U.S. Department of Transportation's New Policy on Automated Vehicles Adopts SAE International's Levels of Automation for Defining Driving Automation in On-Road Motor Vehicles," *SAE international*, p. 1, 2016.
- [2] Tesla, "Impact Report," tech. rep., Tesla, California, 2019.
- [3] National Coordination Office for Space-Based Positioning, Navigation, and Timing, "GPS Accuracy," 2020.
- [4] C. Händel, H. Konttaniemi, and M. Autio寧emi, "State-of-the-Art Review on Automotive Radars and Passive Radar Reflectors," tech. rep., Lapland University of Applied Sciences, 2018.
- [5] H. H. Meinel and J. Dickmann, "Automotive radar: From its origins to future directions," *Microwave Journal*, vol. 56, no. 9, pp. 24–40, 2013.
- [6] K. Yoneda, N. Hashimoto, R. Yanase, M. Aldibaja, and N. Suganuma, "Vehicle Localization using 76GHz Omnidirectional Millimeter-Wave Radar for Winter Automated Driving," *IEEE Intelligent Vehicles Symposium, Proceedings*, vol. June, no. Iv, pp. 971–977, 2018.
- [7] E. Ward and J. Folkesson, "Vehicle localization with low cost radar sensors," *IEEE Intelligent Vehicles Symposium, Proceedings*, vol. August, no. Iv, pp. 864–870, 2016.
- [8] R. Zhang, *MMwave Radar: Enhancing Resolution, Target Recognition, and Fusion with Other Sensors*. PhD thesis, The University of Arizona, 2019.
- [9] P. Asuzu and C. Thompson, "Road condition identification from millimeter-wave radar backscatter measurements," *IEEE Radar Conference, RadarConf*, pp. 12–16, 2018.
- [10] V. Viikari, T. Varpula, and M. Kantanen, "Automotive radar technology for detecting road conditions. backscattering properties of dry, wet, and icy asphalt," *European Radar Conference Proceedings*, pp. 276–279, 2008.
- [11] S. Carpenter, "Autonomous Vehicle Radar: Improving Radar Performance with Simulation," Tech. Rep. 1, ANSYS, 2018.
- [12] U. R. Fawwaz T. Ulaby, *Fundamentals of Applied Electromagnetics*. London: Pearson Education, 2015.
- [13] B. Weidenfeller, M. Höfer, and F. Schilling, "Thermal and electrical properties of magnetite filled polymers," *Composites Part A: Applied Science and Manufacturing*, vol. 33, no. 8, pp. 1041–1053, 2002.
- [14] T. Ghigna, M. Zannoni, M. E. Jones, and A. Simonetto, "Permittivity and permeability of epoxy-magnetite powder composites at microwave frequencies," *Journal of Applied Physics*, vol. 127, no. 4, p. 045102, 2020.
- [15] V. Hoffmann, M. Knab, and E. Appel, "Magnetic susceptibility mapping of roadside pollution," *Journal of Geochemical Exploration*, vol. 66, no. 1-2, pp. 313–326, 1999.
- [16] F. J. McVea, *Electrical properties of the Athabasca tar sands*. PhD thesis, University of Alberta, 1978.
- [17] E. J. Jaselskis, J. Grigas, and A. Brilungas, "Dielectric Properties of Asphalt Pavement," *Journal of Materials in Civil Engineering*, vol. 15, no. 5, pp. 427–434, 2003.
- [18] R. Kishore, "Electrical conductivity of metals," *Physica Status Solidi (B)*, vol. 26, no. 1, pp. 133–138, 1968.
- [19] F. Chen and R. Balieu, "A state-of-the-art review of intrinsic and enhanced electrical properties of asphalt materials: Theories, analyses and applications," *Materials and Design*, vol. 195, p. 109067, 2020.
- [20] OPSS, "Construction Specification for Pavement Marking," Tech. Rep. November, Ontario Provincial Standard Specification, 2010.
- [21] K. Cousino, "Awr1642: Calculating approximate receive power from peakval."